In situ synthesis of Pt nanoparticles in SBA-15 by encapsulating in modified template micelles: size restricted growth within the mesochannels†

Atul K. Prashar,[a] Robert P. Hodgkins,‡[b] Rajiv Kumar[a] and R. Nandini Devi*[a]

Received 21st November 2007, Accepted 7th February 2008
First published as an Advance Article on the web 28th February 2008
DOI: 10.1039/b717991j

A truly *in situ* and simple method is developed for nanoparticle incorporation within the mesochannels of SBA-15 involving dispersion of metal precursors in surfactant-modified polymer micelles. The diffusion of the precursor within the micellar structure is aided by interaction with the cationic head group of the surfactant leading to a unique method to facilitate the formation of highly disperse, uniform nanoparticles molded by the walls of the mesochannels. The nanoparticle incorporated mesoporous material has a highly enhanced surface area and adsorption capabilities in comparison to its parent materials without any pore blockage which makes this method ideal for the preparation of nanocatalysts.

Introduction

In catalysis, dispersion and hence size and morphology of active metals play an important role in overall performance, activity and selectivity of the catalysts.[1–3] Here the ability to stabilize active metals in nano form as well as fine tune the size is paramount to achieving desired performance markers for the catalyst. Even though engineering metal nanoparticles with different sizes and morphologies is very well established now,[4–6] it has been difficult to translate these advances into successful application in catalysis. The main drawback is the possibility of agglomeration and sintering of the nanoparticles under harsh catalytic reaction conditions since they are usually stabilized in organic moieties[7,8] like capping agents and protective polymers. Hence it is imperative to support the nanoparticles effectively on solid and stable materials which would aid to minimize such deactivation processes. In conventional catalyst preparation methods, metal particles are stabilized on the surface and within the macropores of oxide supports just by adsorption of precursor ions and subsequent reduction. In spite of poor control of particle size, these methods are widely followed due to the ease of preparation in large scale syntheses.

However, the advent of mesoporous compounds like SBA-15, MCM-41[9–11] *etc.* has led to exciting forays into their utilization as supports for metal nanoparticles.[12,13] The advantage is the highly porous interpenetrating channel systems without any capillary effect diffusion limitations, thereby increasing the surface area, within which nanoparticles can be located. This is expected to give better control of particle size, morphology and even modified surface properties which can be exploited for various applications even beyond catalysis.[14] Incorporation of metal particles into mesoporous compounds is usually achieved by simply adding metal salt precursors to the oxide precursor sol–gel mixture[15] or wet impregnation of metal salt on already formed mesoporous compounds.[16] These methods have the disadvantage of uncontrolled growth of metal particles on the walls since no preventive measures are taken to ensure that the metal precursors are solely isolated within the channels. Further, grafting of the inner walls of the siliceous materials with functional groups which would preferentially attach metal precursors is also used,[17] but complicated procedures need to be followed to prevent external surface adsorption of the functional group and hence uncontrolled growth of metal particles. Recently, pre-synthesized metal nanoparticles capped by protective agents have been successfully incorporated into the mesochannels exclusively, through wet impregnation or capillary inclusion.[18,19] However, careful surface modification and pore engineering of the host material is necessary to facilitate improved guest uptake. In addition there is a significant reduction in pore volume and surface area in the resulting hybrid material reducing the efficiency.[20] Somarjai and co-workers reported another elegant method in which Pt colloidal solution is prepared and stabilized in a capping agent polyvinylpyrrolidone (PVP) and encapsulated within the SBA-15 silica framework.[21] However, in such a method, highly acidic synthetic precursors of SBA-15 can be detrimental to the stability of the metal colloid and hence careful alterations need to be carried out to the mesoporous materials' synthesis so that the nanoparticles are stable. At this juncture, it would be worthwhile exploring better and simpler methodologies for localizing metal nanoparticles exclusively within the mesochannels while retaining high surface areas and pore volumes—ideal for catalysis amongst other applications.

In our attempts to have better control over the size, amount and location of Pt particles in SBA-15, we have developed a simple and convenient *in situ* method of dispersing the metal salt precursors within template polymers modified with ionic surfactants in a controlled manner. The ionic surfactants are

---

[a] *Catalysis Division, National Chemical Laboratory, Pune 411008, India. E-mail: nr.devi@ncl.res.in*
[b] *Materials Chemistry Research Group, Department of Physical, Inorganic and Structural Chemistry, Arrhenius Laboratory, Stockholm University, SE-106 91 Stockholm, Sweden*

† Electronic supplementary information (ESI) available: Additional XRD and TEM images, pore size and pore volume calculations, catalytic conversion–selectivity data, chemical analysis details. See DOI: 10.1039/b717991j

‡ Present Address: Nanologica AB, Uppsala Innovation Centre, Uppsala Science Park, SE-751 83 Uppsala, Sweden

expected to be dispersed within the polymer micelle structure with the ionic head groups decorating the corona and the hydrophobic tail groups penetrating the core. Added to this polymer–surfactant composite, metal precursor ions diffuse into the corona depending on various factors *viz*. ageing time, surfactant and precursor concentration *etc*. Later calcination of this material leads to a highly homogeneous dispersion of metal nanoparticles of fairly uniform size distribution. This method provides an easy and efficient way to have enhanced control over fine tuning of the particle sizes at the same time ensuring that all nanoparticles are localized within the meso-channels. Further, the textural properties like pore size/volume, surface area *etc*. are observed to be highly enhanced when compared to metal incorporation without the surfactant modification. We explain in this manuscript the methodology adopted in the synthesis of Pt incorporated SBA-15, its characterization and correlation with catalytic activity.

Experimental section

Synthesis

SBA-15 was first prepared using polymer–surfactant composite with varying concentrations of cetyl trimethyl ammonium bromide (CTAB). Typically, 0.0364 g CTAB (LobaChemie) was added to 100 g of 1 wt% solution of block copolymer Pluronic P123 (Aldrich) so that the final composition was 1 mM of CTAB and this mixture was stirred for 12 h at 25 °C. This solution was made acidic ($\text{pH} < 2$) by 6.25 mL conc. HCl (37 %) and 2.08 g tetraethylorthosilicate (TEOS; Aldrich) added under stirring. Stirring was continued for another 24 h at 40 °C and then autoclaved at 90 °C for 48 h. The product was filtered, washed, dried and calcined at 500 °C enabling the template removal. The CTAB concentration was progressively increased to 32 mM in 1 wt% P123 for other samples. For Pt incorporation, 2.4 mL of 1 wt% solution of H_2PtCl_6 (Aldrich) was added to the polymer–surfactant composite solution containing 1 mM CTAB and 1 wt% P123 and stirred for 24 h prior to the addition of conc. HCl and TEOS. The final molar composition of the gel was 1 TEOS : 585 H_2O : 6.3 HCl : 0.017 P123 : 0.01 CTAB : 0.006 H_2PtCl_6. The same procedure as above was followed.

Characterization

Powder X-ray diffraction of all the samples was carried out in a PANalytical X'pert Pro duel goniometer diffractometer. A proportional counter detector was used for low angle experiments and an X'celerator solid state detector was employed in wide angle experiments. The radiation used was Cu Kα (1.5418 Å) with a Ni filter and the data collection was carried out using a flat holder in Bragg–Brentano geometry (0.5 to 5°; 0.2° min^{-1}). Care was taken to avoid sample displacement effects. A JEOL JEM-3010 operating at 300 kV (Cs = 0.6 mm, resolution 1.7 Å) was used for HRTEM sample observation. A Gatan digital camera (model 794, Gatan 1024 × 1024 pixels, pixel size 24 × 24 µm) at 15 000–80 000× magnifications was used to record micrographs. Samples were crushed, dispersed in ethanol before depositing onto a holey carbon grid. Nitrogen adsorption–desorption isotherms were acquired using a Micromeritics ASAP 2020 instrument. The program consisted of both an adsorption and desorption branch and typically ran at −196 °C after samples were degassed at 120 °C for 2 h once the final temperature had been maintained. Specific surface areas were calculated *via* the BET model at relative pressures of $P/P_0 = 0.06$–0.3. The total pore volume was estimated from the uptake of adsorbate at a relative pressure of $P/P_0 = 0.99$. Pore size distribution curves were obtained *via* the NLDFT model assuming cylindrical pore geometry and the micropore volume calculated *via* *t*-plot analyses as a function of relative pressure using the Broekhoff de Boer model for thickness curves measured between 3.5–5.0 Å. Chemical anaysis was carried out in a LabTam 8440 Plasmalab sequential mode ICP-AES spectrometer. The samples were dissolved in *aqua regia* and the undissolved siliceous matter filtered off prior to analysis. Catalytic activity of the Pt incorporated sample was tested for hydrogenation of cinnamaldehyde. A 100 mL stainless steel reactor equipped with a pressure gauge, stirrer and thermocouple was used as the reaction vessel. 1.25 g of cinnamaldehyde in 20 mL of isopropanol was charged in the reactor and heated to 80 °C under a H_2 pressure of 2.96 MPa. At intervals, aliquots of the reaction mixture were taken from the reactor and GC analysis performed on Agilent Technologies 6890 N Network GC system using a HP5 column.

Results

Modifying polymer micelles with surfactants is expected to facilitate metal precursor diffusion by interaction with the ionic head groups.[22] However, polymer–surfactant interaction can affect the micelle structure in many ways.[23–25] These changes, in turn, will be reflected in the final mesoporous structure.[26] SBA-15 was synthesized with varying amounts of the surfactant, CTAB in the polymer P123 and powder XRD studies were carried out to follow the effects as shown in Fig. 1. At 1 mM CTAB, the mesoporous structure with long range order remains intact as shown by the higher angle peaks, albeit with a negligible contraction. Thus it becomes evident that the presence of CTAB at this concentration within the polymer micelle has no effect on the overall micellar structure. However, as CTAB concentration is increased to 4 mM, there is a contraction of the unit cell and

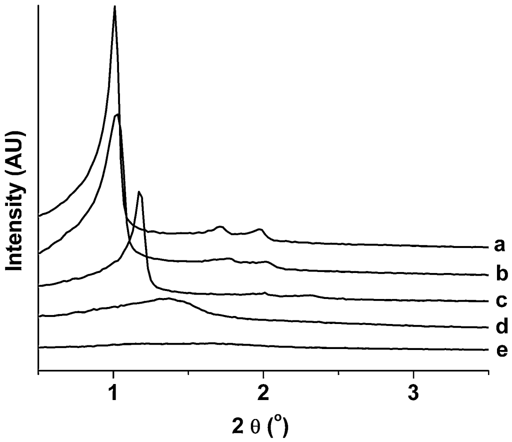

Fig. 1 Comparison of XRD patterns of SBA-15 prepared using 1 wt% P123 and varying amounts of CTAB: (a) no CTAB, (b) 1 mM CTAB, (c) 4 mM CTAB, (d) 16 mM CTAB and (e) 32 mM CTAB.

the long range order starts decreasing. Any further increase in CTAB concentration results in a collapse of the structure since the micellar structure is completely destroyed.

Our intention was to optimize the concentration of the surfactant CTAB which can be dispersed within the polymer micelle without altering the micellar structure, under which conditions the ionic head group of the surfactant will decorate the corona (Scheme 1). Hence an optimum final concentration of 1 mM CTAB was selected for further studies. When added to this composite, $[PtCl_6]^{2-}$ will interact with the cationic head groups of CTAB and disperse effectively in the corona at the ethylene oxide (EO)–propylene oxide (PO) interface inside the micelle. The hydrophobic hydrocarbon of the surfactant will reside in the PO core of the micelle while the cationic head group will reside at the EO–PO interface. The concentration of platinum was fixed at 0.06 mM so that the Pt loading will be 1–2 wt% in the final mesoporous compound. Pt incorporation did not have any effect on the formation of SBA-15, retaining the long range order. The XRD studies further showed that a discernible expansion of the mesoporous unit cell occurred by the inclusion of Pt when compared to the mesoporous material prepared without platinum dispersion (Fig. 2). Scanning at high angles revealed the presence of Pt nanoparticles of ~8 nm calculated by the Scherrer equation. A small swelling of the material with Pt before calcination was also observed (see ESI†) pointing to a possible effect by the mere dispersion of the Pt precursor within the template on the unit cell.

Very interestingly, N_2 adsorption studies showed that the Pt incorporation has led to an unusual increase in surface area and overall adsorption capability when compared to pure and CTAB modified SBA-15 (Table 1). The shape of the isotherm of Pt/SBA-15 also remained unchanged indicating the absence of any blockage of the channels by the Pt nanoparticles (Fig. 3). The adsorption properties of Pt/SBA-15 are enhanced compared to pure SBA-15. The surface area increases by 60%, pore volume by 56%, adsorbate uptake by 57% and the mode pore diameter by 22%. This is consistent with the unit cell expansion as seen by XRD studies and further suggests that the Pt

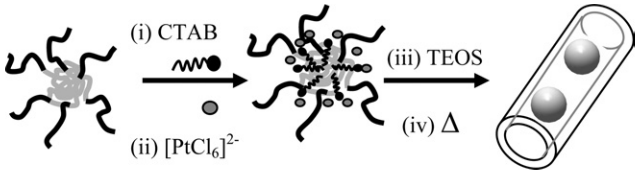

Scheme 1 Ensuring the formation of nanoparticles within the mesochannels by dispersing metal precursors in surfactant-modified polymer micelles

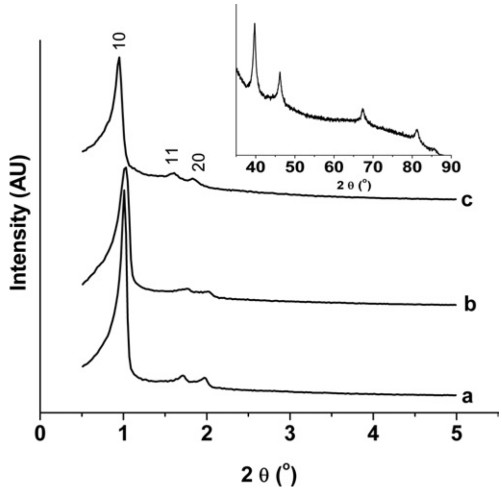

Fig. 2 XRD patterns of calcined samples: (a) pure SBA-15 using 1 wt% P123 as template, (b) SBA-15 with 1 mM CTAB incorporated into 1 wt% P123 and (c) Pt incorporated SBA-15 prepared with 1 wt% polymer template P123 and 1 mM CTAB. Inset: Wide angle XRD showing the presence of Pt nanoparticles of average size ~8 nm calculated by the Scherrer equation.

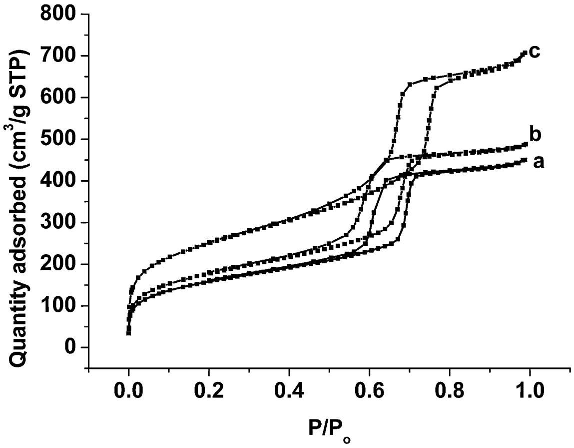

Fig. 3 N_2 adsorption isotherms of (a) pure, (b) CTAB added and (c) Pt/CTAB incorporated SBA-15.

Table 1 Unit cell and adsorption measurements of calcined samples: pure SBA-15, SBA-15 (with CTAB) and Pt-SBA-15 (with CTAB)

Material	Unit cell[a]/Å	Pore size[b]/Å	BET[c]/m^2 g^{-1}	N_2 uptake/cm^3 g^{-1} STP	Total pore volume[d]/cm^3 g^{-1}	Micropore volume[e]/cm^3 g^{-1}
Pure SBA-15	99	87	550 ± 5.0	451	0.70	0.03
SBA-15 (with CTAB)	98	83	621 ± 5.2	489	0.75	0.02
Pt-SBA-15 (with CTAB)	108	106	870 ± 7.4	707	1.09	0.04

[a] Hexagonal lattice parameter: $a = \sqrt{4/3}\ d_{10}$. [b] Pore size distribution calculated on the adsorption branch of the isotherm *via* the DFT model assuming cylindrical pore geometry. [c] BET specific surface area calculated within relative pressures of $P/P_0 = 0.06$–0.3. [d] Total pore volume measured at a relative pressure of $P/P_0 = 0.99$. [e] Calculated through *t*-plot analysis as a function of relative pressure using the Broekhoff de Boer model for thickness curve measured between 3.5 and 5 Å: $\log(P/P_0 = -16.11/t^2 + 0.1682\exp(-0.1137t)$.

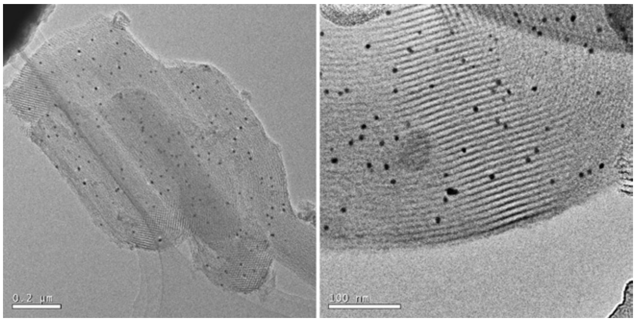

Fig. 4 TEM images of Pt incorporated SBA-15 showing a uniform dispersion of nanoparticles. The particles are localized within the pores, grown within and molded by the channel walls. The average particle size is measured to be 6–8 nm.

precursors reside within the corona (EO–PO interface) of the micelles during the synthesis.

TEM images of the final calcined sample show a very uniform dispersion of Pt particles within the SBA-15 framework. A general scan of the sample did not show any Pt particles on the surface of the silica matrix, as expected (Fig. 4). A closer look at the mesochannels evidenced the presence of nanoparticles of an average size 6–8 nm, located well within the mesopores molded by the walls of the channels. It also becomes clear from TEM that some of the nanoparticles may lead to localized swelling of the mesopore wall structure probably because the local concentration of the precursor exceeded the optimum for restricted growth within the channel (ESI†). It is noteworthy that most of the particles have grown within the channels and no sign of agglomeration is seen. This shows that the Pt precursor could diffuse well into the micelle structure aided by the attractive force towards the ionic head group in the corona, preventing the formation of clusters of Pt precursor which would later lead to metal particle agglomeration. To confirm the role of CTAB in enhancing precursor dispersion, SBA-15 was prepared by using $[PtCl_6]^{2-}$/P123 composite as a template without CTAB addition and the final calcined material observed under TEM. In this case, agglomeration of Pt over the surface of the mesoporous material was seen (see ESI†). The retention of Pt was also highly improved (40%) in CTAB incorporated polymer when compared to naked micelle (7%). TEM images of the uncalcined sample showed only traces of Pt particles (see ESI†).

Further understanding of the surface structure and morphology of the Pt nanoparticles, however, could not be achieved by TEM since they are situated in the channels encapsulated by the silica wall. Under such conditions, probe reactions utilizing multifunctional molecules are proposed to be ideal tools to give insight into the selectivity and in turn surface properties of active metal nanoparticles. Selective hydrogenation of α,β-unsaturated aldehydes is well studied and structure–selectivity correlations well established. Hence catalytic activity of the Pt/SBA-15 was tested for hydrogenation of cinnamaldehyde (Fig. 5) and selectivity studied by following the formation of cinnamyl alcohol, hydrocinnamaldehyde and phenyl propanol by gas chromatography (see ESI†). The selectivity towards cinnamyl alcohol increased with reaction duration and reached a maximum at 3 h. Hydrocinnamaldehyde selectivity also increased initially but decreased rapidly after 1 h as complete hydrogenation to phenylpropanol started to occur. Hence the hydrogenation of the terminal aldehyde group was preferred over the alkene group forming the desired product. It is interesting to note here that the particles remained stable without sintering retaining the well-defined mesostructure of the catalyst after the reaction (Fig. 6).

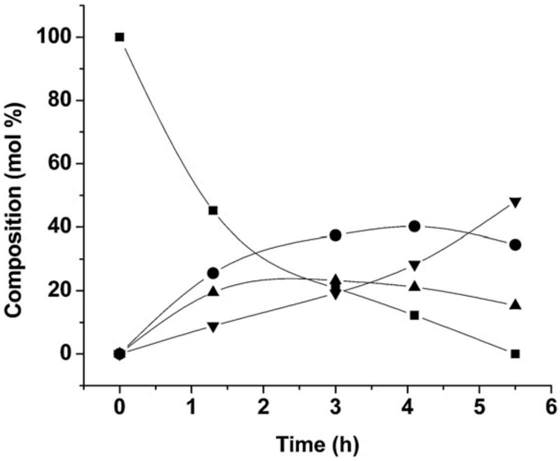

Fig. 5 Cinnamaldehyde hydrogenation activity of Pt/SBA-15 (■ cinnamaldehyde; ● cinnamyl alcohol; ▲ hydrocinnamaldehyde; ▼ phenylpropanol).

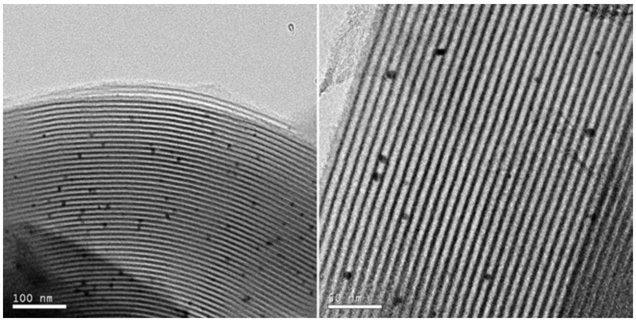

Fig. 6 TEM images of the Pt sample after catalytic testing. The particle size remains on average 6–8 nm without agglomeration.

Discussion

XRD studies of SBA-15 prepared from composites with different concentrations of CTAB in polymer P123 indicated a clear effect of the surfactant on the micelle and hence the mesoporous structure. At lower concentrations of surfactant, the interaction is cooperative whereby the hydrophobic tail of the surfactant is anchored to the core and the ionic head group dispersed in the corona of the polymer micelle. However, it is possible that at higher concentrations, the polymer micelle gradually monomerises to a "necklace" structure in which the surfactant groups decorate the individual strands of the polymer.[27] Selection of the cooperative composite structure is crucial for two reasons: (1) at low concentrations, addition of the surfactant does not disturb the overall micelle structure and hence ensures the formation of the desired mesoporous material with continued long range order; (2) modifying polymers with surfactants in this way is ideal for metal precursor dispersion since the positively charged head group of CTAB facilitates the diffusion of negatively charged $[PtCl_6]^{2-}$ ions. During the formation of the mesoporous compound, the silica precursor species assemble around the micelle template leading to the interconnecting channels with siliceous walls. Thus, the cooperative surfactant polymer composite with Pt precursor well dispersed in the corona ensures the encapsulation of the metal species within the channels of the final mesoporous compound. Without the surfactant additive to aid proper dispersion of the precursor, agglomeration of the Pt species occurs which later leads to bigger particles on calcination. XRD, TEM, adsorption and catalytic studies have thrown light upon the possible mechanisms of formation of the Pt nanoparticles within the mesochannels and the effect on the overall physical properties of the metal incorporated SBA-15. We observe a small swelling of the mesoporous material upon dispersion of the Pt precursor in the surfactant (as shown by the XRD of the uncalcined sample). This can probably be attributed to an overall swelling of the corona due to the repulsion among the cationic head groups, now enhanced by the presence of the $[PtCl_6]^{2-}$ ions. This in turn increases the micelle volume and leads to a subsequent increase in the unit cell and pore size upon calcination. This expansion in the unit cell and pore size gives strong evidence that the silica walls expand to incorporate the Pt salts/nanoparticles within the micellar structure. Incorporation of Pt apparently results in a decrease in the siliceous wall thickness which could be due to either a dampened interaction of the micelle with the silica precursor in the presence of Pt salt or an effect of nanoparticle formation during calcination. However, it is worth noting that this decrease did not have any effect on the long range of the mesostructure even after the hydrogenation reaction. Moreover, TEM images show a widening of the channels, albeit locally, during the formation of nanoparticles. Since only traces of Pt nanoparticles were observed in the uncalcined sample, we can deduce that the temperature and duration of the synthetic procedure is enough for partial formation of the particles but calcination can be concluded as the final step of size restricted growth of the nanoparticles.

Cinnamaldehyde hydrogenation is used as a probe for better understanding the surface morphology of the nanoparticles. This reaction proceeds through a parallel and consecutive mechanism by reduction of C=C and C=O bonds. Particle size is reported to play a commanding role in deciding selectivity towards unsaturated alcohol or saturated aldehyde;[28] as particle size increases (5–9 nm), C=O hydrogenation is more favoured. This is due to the extent of exposure of different crystallographic planes with increasing particle size. Selectivity arises here due to differences in adsorption energies of C=O and C=C on different crystallographic planes of Pt. Hydrogenation of C=O to give unsaturated alcohol is proposed to be faster on the Pt(111) plane whereas Pt(110) facilitates C=C adsorption and hence formation of saturated aldehyde selectively.[29,30] We utilized this fact for further probing the characteristics of the nanoparticle. Change in activity and selectivity depending on particle sizes has been reported for Pt based catalysts on different supports.[31,32] 3 wt% Pt supported on carbon nanotubes, for instance, showed ~33% increase in selectivity of cinnamyl alcohol over hydrocinnamaldehyde when the particle size increased from 2 to 5 nm. The title compound, Pt-SBA-15 showed a maximum selectivity of 53% for cinnamyl alcohol at a conversion of 65%. This high selectivity towards C=O hydrogenation is in accordance with the reported observations indicating an abundance of exposed (111) planes in the Pt nanoparticles with sizes of the order of 6–8 nm.

The stability of nanoparticles is a well debated requirement in relation to catalytic processes due to deactivation caused by metal sintering. Localization of the nanoparticles exclusively within the channels of SBA-15 clearly deters the agglomeration of nanoparticles when exposed to aggressive conditions. Along with this advantage, the ease of incorporation of metal nanoparticles into the mesostructured matrix makes the reported method ideal for nanocatalyst synthesis. Furthermore, this method for Pt nanoparticle incorporation using a simple *in situ* method from metal precursors makes the material ideal for host–guest relationships with minimal diffusion limitations over a large surface when compared to the methods previously described.

Conclusion

A novel yet convenient method of synthesis is developed for incorporating Pt nanoparticles into mesoporous SBA-15. The methodology exploits the electrostatic interaction between metal precursor salts and the ionic surfactant head groups incorporated into the polymer micelle in a controlled manner. The cooperative interaction of the hydrophobic tail group of the surfactant with the hydrophobic core of the micelle so that the ionic head groups decorate the corona without altering the micellar structure is paramount for the formation of well-ordered SBA-15 as well as uniform dispersion of the Pt precursor. Structural characterization by diffraction, microscopy and adsorption studies point to an exclusive localization of Pt nanoparticles within the mesochannels leading to a material with enhanced physical properties like adsorption capacity, surface area and pore volume. Pt nanoparticles of size 6–8 nm were observed uniformly dispersed and located inside the mesochannels. Furthermore, incorporation of CTAB and later Pt precursor seems to alter the relative pore characteristics resulting in a material superior to the parent compounds. Moreover, most advantageously, the nanoparticles are unaltered and not sintered after catalytic reactions. Hence this method can be utilized in nanocatalysis more effectively: added advantages being the ease of preparation as well as the localization of the nanoparticles within the channels. Since proper diffusion of the metal precursor is crucial to nanoparticle formation, we believe that fine tuning of the particle size is quite plausible with control in synthesis conditions. A concerted study of these materials in different stages and under various conditions of preparation is underway to further understand the exact mechanism of formation of the nanoparticles.

Acknowledgements

AKP acknowledges CSIR, New Delhi, India for fellowship and RPH through Prof. Lennart Bergström, Stockholm University, thanks the Swedish Research Council (VR) for funding. We thank RSIC, IIT Mumbai, India for ICP analysis.

References

1 G. A. Somorjai and Y. G. Borodko, *Catal. Lett.*, 2001, **76**, 1.
2 R. M. Rioux, H. Song, M. Grass, S. Habas, K. Niesz, J. D. Hoefelmeyer, P. Yang and G. A. Somorjai, *Top. Catal.*, 2006, **39**, 167.
3 L. Guczi, G. Peto, A. Beck and Z. Paszti, *Top. Catal.*, 2004, **29**, 129.
4 J. Park, K. An, Y. Hwang, J.-G. Park, H.-J. Noh, J.-Y. Kim, J.-H. Park, N.-M. Hwang and T. Hyeon, *Nat. Mater.*, 2004, **3**, 891.
5 M. P. Pileni, *J. Phys. Chem. C*, 2007, **111**, 9019.
6 D. Kim, J. Park, K. An, N.-K. Yang, J.-G. Park and T. Hyeon, *J. Am. Chem. Soc.*, 2007, **129**, 5812.
7 S. Ozkar and R. G. Finke, *J. Am. Chem. Soc.*, 2002, **124**, 5796.
8 N. Toshima, Y. Shiriashi, T. Teranishi, M. Miyake, T. Tominaga, H. Watanabe, W. Brijoux, H. Bonnemann and G. Schmid, *Appl. Organomet. Chem.*, 2001, **15**, 178.
9 D. Y. Zhao, Q. Huo, J. Feng, B. F. Chmelka and G. D. Stucky, *J. Am. Chem. Soc.*, 1998, **120**, 6020.
10 D. Y. Zhao, J. Feng, Q. Huo, N. Melosh, H. G. Fredrickson, B. F. Chmelka and G. D. Stucky, *Science*, 1998, **279**, 548.
11 C. T. Kresge, M. E. Leonowicz, W. J. Roth, J. C. Vartuli and J. S. Beck, *Nature*, 1992, **359**, 710.
12 K. Moller and T. Bein, *Chem. Mater.*, 1998, **10**, 2950.
13 H. Li, J. Chen, Y. Wan, W. Chai, F. Zhang and Y. Lu, *Green Chem.*, 2007, **9**, 273.
14 L. M. Bronstein, *Top. Curr. Chem.*, 2003, **226**, 55, and references therein.
15 R. S. Mulukutla, K. Asakura, T. Kogure, S. Namba and Y. Iwasawa, *Phys. Chem. Chem. Phys.*, 1999, **1**, 2027.
16 M. H. Haung, A. Choudrey and P. Yang, *Chem. Commun.*, 2000, 1063.
17 Z. Zhang, S. Dai, X. Fan, D. A. Blom, S. J. Pennycook and Y. Wei, *J. Phys. Chem. B*, 2001, **105**, 6755.
18 Z. Kónya, V. F. Puntes, I. Kiricsi, J. Zhu, J. W. Ager III, M. K. Ko, H. Frei, P. Alivisatos and G. A. Somorjai, *Chem. Mater.*, 2003, **15**, 1242.
19 P. Mukherjee, M. Sastry and R. Kumar, *PhysChemComm.*, 2004, 4.
20 R. P. Hodgkins, A. Ahniyaz, K. Parekh, L. M. Belova and L. Bergström, *Langmuir*, 2007, **23**, 8838.
21 H. Song, M. R. Rioux, D. J. Hoefelmeyer, R. Komor, K. Niesz, M. Grass, P. Yang and G. A. Somorjai, *J. Am. Chem. Soc.*, 2006, **128**, 3027.
22 L. M. Bronstein, D. M. Chernyshov, G. T. Timofeeva, L. V. Dubrovina, P. M. Valetsky, E. S. Obolonkova and A. R. Khokhlov, *Langmuir*, 2000, **16**, 3626.
23 M. Antonietti, S. Heinz, M. Schmidt and C. Rosenauer, *Macromolecules*, 1994, **27**, 3276.
24 E. Hecht and H. Hoffmann, *Langmuir*, 1994, **10**, 86.
25 J. Jansson, K. Schillen, G. Olofsson, R. Cardoso da Silva and W. J. Loh, *J. Phys. Chem. B*, 2004, **108**, 82.
26 H. W. Zhang, L. Zhang, J. Xiu, Z. Shen, Y. Li, P. Ying and C. Li, *Micropor. Mesopor. Mat.*, 2006, **89**, 179.
27 S. Dai, K. C. Tam and L. Li, *Macromolecules*, 2001, **34**, 7049.
28 P. Gallezot and D. Richard, *Catal. Rev.-Sci. Eng.*, 1998, **40**, 81.
29 F. Delbecq and P. J. Sautet, *J. Catal.*, 1995, **152**, 217.
30 B. Coq and F. Figueras, *Coordin. Chem. Rev.*, 1998, **178**, 1753.
31 D. Manikandan, D. Divakar and T. Sivakumar, *Catal. Commun.*, 2007, **8**, 1781.
32 H. Ma, L. Wang, L. Chen, C. Dong, W. Yu, T. Huang and Y. Qian, *Catal. Commun.*, 2007, **8**, 452.